Supporting Information

Enhanced electrical properties at boundaries including twin boundaries of polycrystalline CdTe thin-film solar cells

H. Li,[a,b] X. X. Liu,[a,b]* Y. S. Lin,[b] B. Yang, [a,b] Z. M. Du[a,b]

[a]The Key Laboratory of Solar Thermal Energy and Photovoltaic System, Institute of Electrical Engineering, Chinese Academy of Sciences, Beijing 100190, China

[b]Institute of Electrical Engineering, Chinese Academy of Sciences, Beijing 100190, China

*Corresponding author email address: shinelu@mail.iee.ac.cn

Device Procedure:

The CdTe solar cell devices were fabricated by a radio-frequency magnetron sputtering method. The 100 nm O:CdS was deposited at room temperature onto an NSG14 commercial glass. The CdTe was deposited on the O:CdS surface at 270 ºC. Cl treatment was conducted at 400 ºC for 60 min in a $CdCl_2$ and dry-air atmosphere. The CdS/CdTe growth conditions are listed in Table S1. The 4 nm Cu was evaporated on the Cl-treated CdTe surface without an etching process. At this stage, the Cu diffusion was performed at 170 ºC for 40 min.

Table S1 CdS/CdTe growth conditions.

Thin film	Base Pressure (Pa)	Deposition Pressure (Pa)	Ar (sccm)	O_2 (sccm)	RF power density (W/cm^2)	Substrate Temperature (° C)	Thickness (μm)
CdS	10^{-3}	3	28.3	0.25	0.88	25	0.1
CdTe	10^{-4}	2	28.3	0	1.32	272	2.3

Characterizations: For electron backscatter diffraction (EBSD) sample preparation, an FEI Helio Nano Lab Nova200 Dual Beam system (FEI Company, Hillsboro, OR USA), equipped with both electron and focused Ga+ ion beams (FIB) was used to cut a flat analysis plane at 1.5º to the surface prior to EBSD. A mill box of 30 μm × 20 μm ×1.5 μm was positioned on the film surfaces and milled at 30 kV beam energy and 1 nA of beam current for an approximate milling time of 10 min. The EBSD was conducted in an FEI XL-30 FEG scanning electron microscope (SEM) equipped with an EDAX-TSL Hikari EBSD detector running OIM Data Collection version 5.32. The EBSD patterns were collected at 20 kV with an approximate beam current of 3 nA at a 13 mm working distance. For mapping, EBSD patterns were automatically collected and analyzed at a rate of 100 points/s from an 18.5 μm×18.5 μm area using a hexagonal sampling grid with 25 nm spacing, resulting in approximately 6.4×10^5 measurements in 107 min. The collected EBSD mapping data were analyzed using EDAX-TSL OIM Analysis version 5.31.

EBSD results: Fig. S1 shows the EBSD grain boundary map of a Cl-treated and Cu-incorporated CdTe film, along with the table of twin boundary (TB) types, fraction, volume, MDF value, number, and length information. In the EBSD grain boundary map, each boundary type is indicated by a different color.

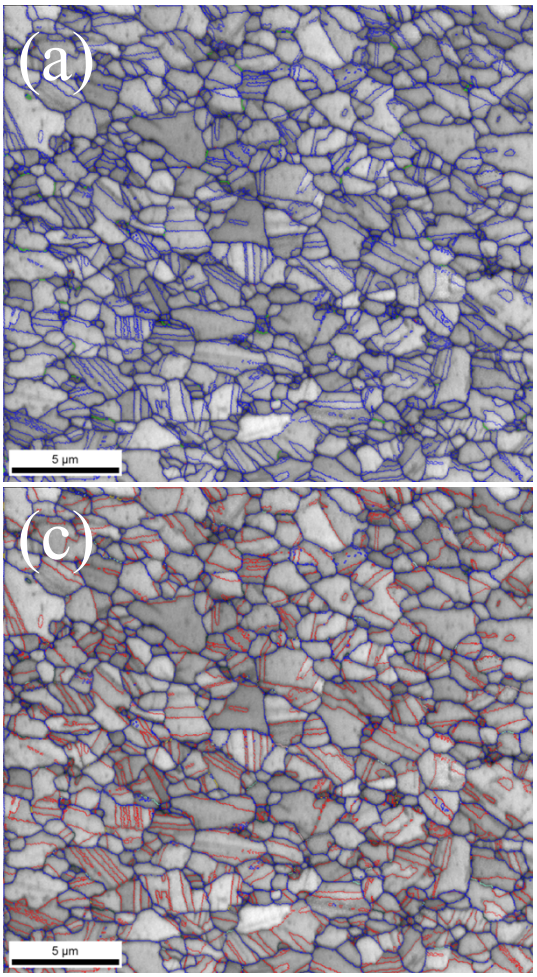

(b)

Gray Scale Map Type:Image Quality
306.153...2147.24 (306.153...2147.24)

Color Coded Map Type: <none>

Boundaries: Rotation Angle

	Min	Max	Fraction	Number	Length
	2°	5°	0.006	525	15.16 microns
	5°	15°	0.014	1175	33.92 microns
	15°	180°	0.980	84525	2.44 mm

*For statistics - any point pair with misorientation exceeding 2° is considered a boundary
total number = 86225, total length = 2.49 mm)

(d)

Boundaries: CSL

	Sigma	Tolerance	Fraction	Volume	MDF Value	Number	Length
	1	15.00	0.020	0.0228	0.87	1700	49.0747 microns
	3	8.66	0.470	0.0176	26.74	40496	1.16902 mm
	5	6.71	0.007	0.0123	0.57	599	17.2916 microns
	7	5.67	0.005	0.0099	0.48	410	11.8357 microns
	9	5.00	0.015	0.0102	1.51	1320	38.1051 microns
	11	4.52	0.006	0.0075	0.83	538	15.5307 microns
	13a	4.16	0.002	0.0029	0.81	205	5.91784 microns
	15	3.87	0.003	0.0094	0.32	257	7.41895 microns
	17a	3.64	0.001	0.0020	0.45	76	2.19393 microns
	19a	3.44	0.002	0.0033	0.71	204	5.88897 microns
	21a	3.27	0.001	0.0019	0.31	50	1.44337 microns
	summary	-	0.532	0.0996	5.34		

Fig. S1. (a) Electron backscatter diffraction (EBSD) grain boundary map of a Cl-treated and Cu-incorporated CdTe film. Blue coloring: boundaries between neighboring lattices differing in orientation by larger angles (15-180°); red coloring: boundaries between neighboring lattices differing in orientation by angles of (2-5°); green coloring: boundaries between neighboring lattices differing in orientation by angles of (5-15°). (b) The table of boundaries types, fraction, volume, MDF value, number, and length information. (c) EBSD grain boundary map of a Cl-treated and Cu-incorporated CdTe film, indicating 53.2% boundaries are CSL boundaries, in which 47.0% are Σ 3 CSL TBs. (d) The table of boundaries types, fraction, volume, MDF value, number, and length information.

Morphology, conductive atomic force microscopy current mapping, and scanning Kelvin probe microscopy measurements: Fig. S2 shows the schematic image for

morphology, conductive atomic force microscopy (C-AFM) current mapping, and scanning Kelvin probe microscopy (SKPM) measurements of CdTe solar cells. The morphology and C-AFM measurements were conducted in a contact mode. For the C-AFM current mapping measurement, the C-AFM tip (SCM-PIT: Si-coated Pt/Ir tip with force constant of 2.8 N/m, frequency of 75 kHz, and diameter of 20 nm) was applied. The SKPM measurement was conducted in a two-step model. The morphology of the CdTe polycrystalline thin film was first obtained in a contact mode; afterward, the conducting tip was lifted from the CdTe surface and held at 100 nm to conduct the SKPM measurement. All SKPM measurements were performed using a Nanoman VS utilizing a dual-pass (interleave) technique in which each single-axis line scan was first recorded in Tapping Mode (TM) to produce the topographic image. The topographic line scan was then used to re-trace the same path in non-contact mode, and at a pre-selected constant height, to obtain computer produced drawing (CPD) signal. By raster scanning over the XY plane, two-dimensional topographic and CPD images were obtained.. By raster scanning over the XY plane, two-dimensional topographic and CPD images were obtained. In the SKPM measurement, the sample was grounded and the DC voltage was applied to the tip. Thus, the contact potential difference is equal to the (Wtip – Wsample)/e, where the Wtip is the work function of tip and the Wsample is the work function of sample.[1]

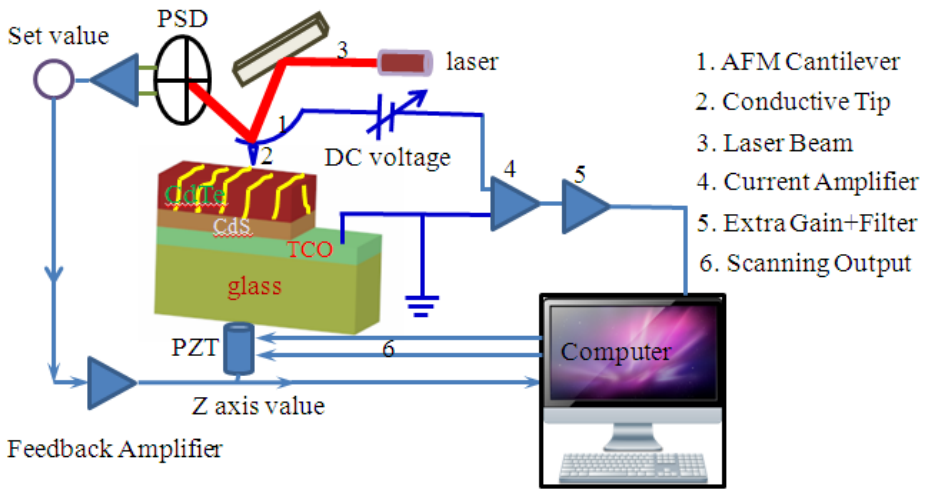

Fig. S2. Schematic image for morphology, conductive atomic force microscopy (C-AFM) current mapping, and scanning Kelvin probe microscopy (SKPM) potential measurements.

CAFM current mapping results: Fig. S3 shows the height-sensor image, deflection-error image, and C-AFM current mapping images of CdTe solar cells with Cl treatment and Cu incorporation. The morphology of CdTe is seen from the height-sensor image. However, the TB information is quite clear in the deflection-error image.

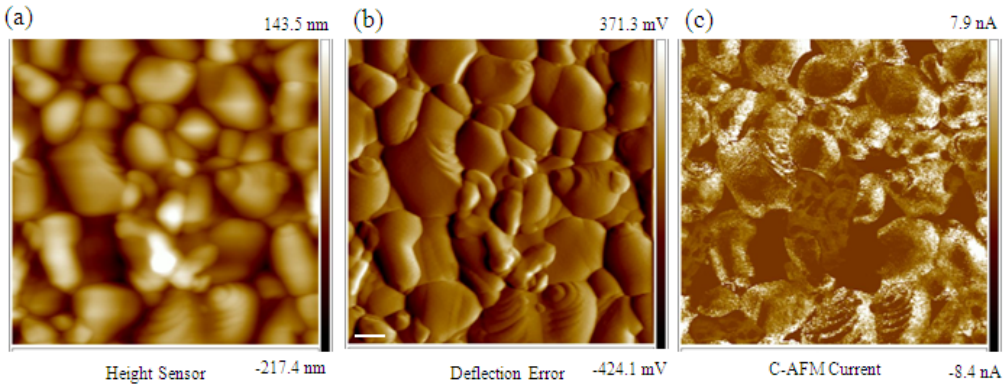

Fig. S3. (a) Atomic force microscopy (AFM) height-sensor image of CdTe surface with twin boundaries (TBs) with Cl treatment and Cu incorporation. (b) AFM deflection-error image of CdTe surface with TBs with Cl treatment and Cu incorporation. (c) Conductive-AFM (C-AFM) current mapping image of CdTe surface with TBs with Cl treatment and Cu incorporation, but with no tip DC voltage and no light. The scale bar is 1 μm.

Scanning electron microscopy results: Fig. S4 shows the scanning electron microscopy (SEM) images of CdTe after Cl treatment and Cu incorporation. From these SEM images, the four types of CdTe grains according to the {111} Σ3 TBs type are clearly seen.

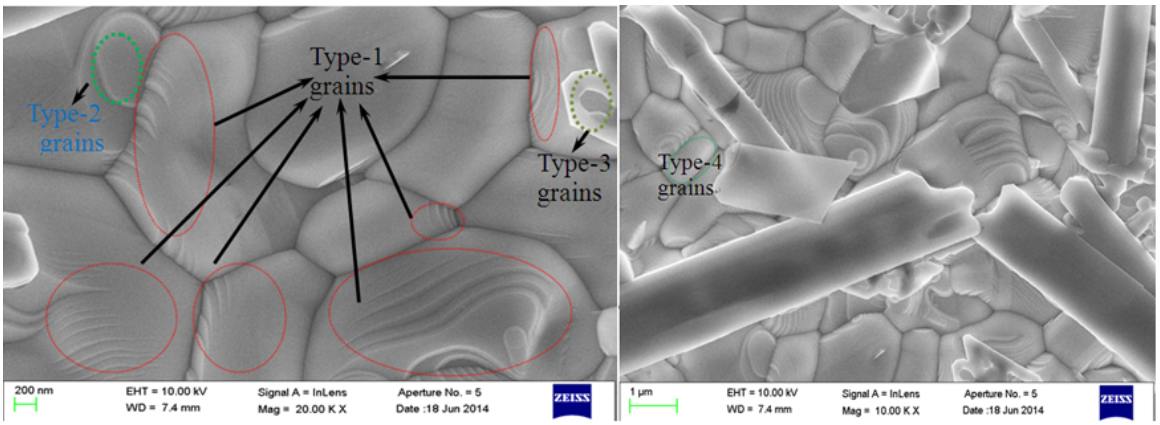

Fig. S4. Scanning electron microscopy (SEM) images of CdTe with Cl treatment and Cu incorporation. The four types of CdTe grains are clearly seen from the SEM images.

SEM and EDXS results: **Fig. S5** shows SEM and EDXS results of CdTe after Cl treatment. There are two type grains: CdTe grains and grains composed of Cl, O, Cd, Te elements located at the grain boundaries of CdTe.

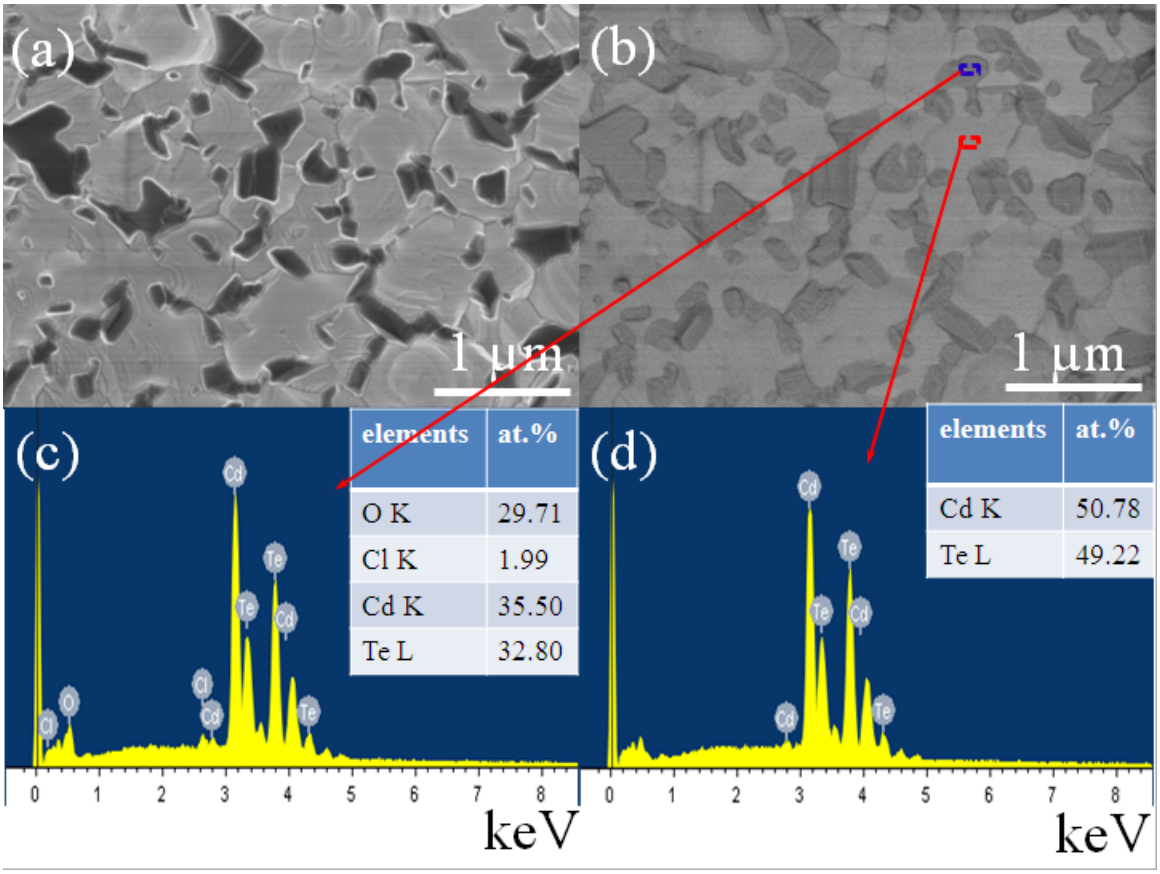

Fig. S5 (a) SEM image of CdTe after Cl treatment. (b) SEM image in back scatter mode of CdTe after Cl treatment, indicating the elements composition difference between grain

interior and grain boundaries. (c) EDXS spectrum of grains distributing at the grain boundaries of CdTe. The inset table shows the elements composition of these grains. (d) EDXS spectrum of the CdTe grains dotted by the dashed rectangular shown in Fig. S5 b. The inset table shows the elements composition.

CAFM current mapping results: Fig. S6 shows the three-channel AFM results for Cl-treated CdTe and Cu incorporation. Fig. S6a shows the AFM height-sensor image of CdTe with Cl-treated and Cu-incorporated. Fig. S6b shows the corresponding C-AFM current mapping image. The grain boundaries enhanced current transport phenomenon is clearly seen. From the section curve along the line in the AFM height-sensor and current mapping images of Cl-treated and Cu-incorporated CdTe (Fig. S6c), the TB-enhanced current transport phenomenon is more clearly seen. Fig. S7 shows AFM height-sensor (Fig. S6a), AFM deflection-error (Fig. S7b), and C-AFM current mapping images (Fig. S7c-h) of CdTe with Cl treatment and Cu incorporation. The C-AFM current mapping images were obtained with tip DC voltages of 0, 0.2, 0.6, 0.8, 1, and 1.2 V. The TBs enhanced current transport phenomenon is clearly seen, in which the Type-2 grains are quite clearly seen. Fig. S8 shows a typical *I-V* curve measured by C-AFM at the CdTe surface. The conductive regions clearly show diode characteristics.

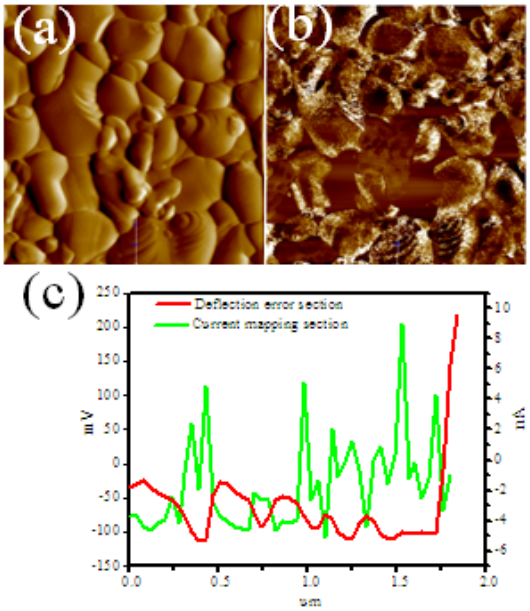

Fig. S6. Three-channel atomic force microscopy (AFM) results for Cl-treated CdTe. (a) AFM height-sensor image of Cl-treated and Cu-incorporated CdTe. (b) Corresponding conductive-AFM (C-AFM) current mapping image of Cl-treated and Cu-incorporated CdTe. (c) Section curve along the line in the AFM height-sensor and current mapping images of Cl-treated and Cu-incorporated CdTe, indicating the TB-enhanced current transport phenomenon.

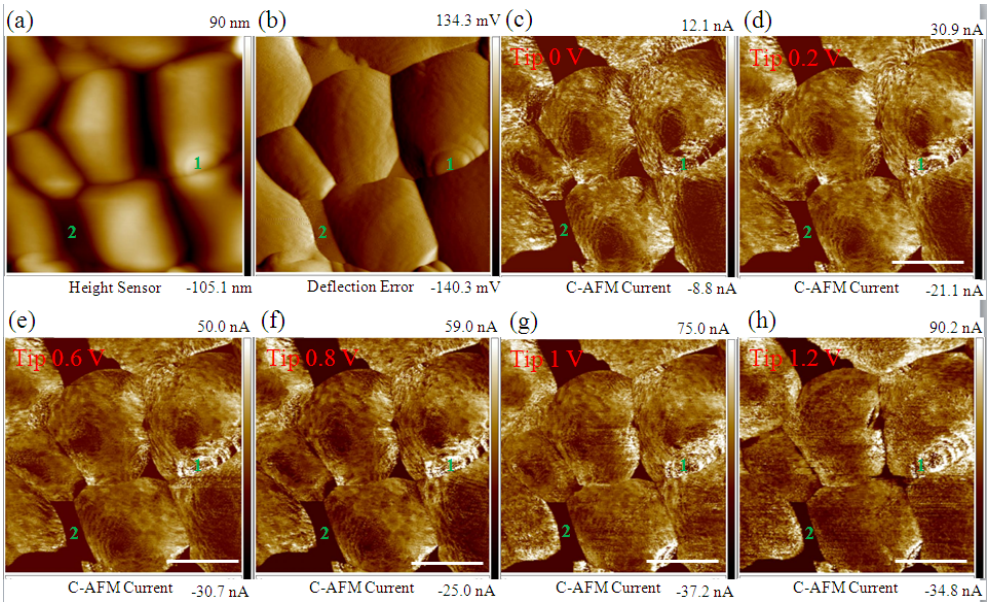

Fig. S7. Three-channel atomic force microscopy (AFM) results for Cl-treated CdTe. (a) AFM height-sensor image of Cl-treated and Cu-incorporated CdTe. (b) Corresponding AFM

deflection-error image of Cl-treated and Cu-incorporated CdTe. (c-h) Corresponding conductive-AFM (C-AFM) current images of Cl-treated and Cu-incorporated CdTe with different tip DC voltages. The tip DC bias was varied from 0 V to +1.2 V. The scale bar is 1 μm.

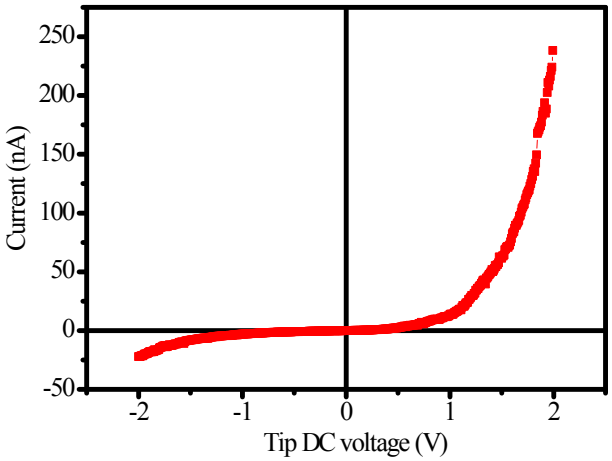

Fig. S8. Typical *I-V* curve as measured by conductive atomic force microscopy (C-AFM) at the CdTe surface.

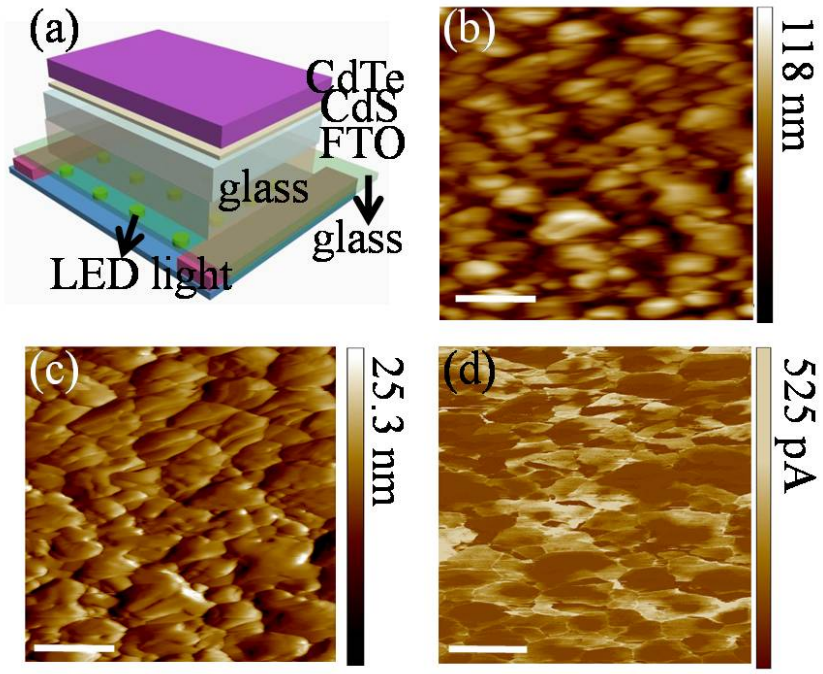

Fig. S9. (a) Sketch of the conductive atomic force microscopy (C-AFM) measurement of the Type-4 CdTe grains. (b) AFM height-sensor image of Cl-treated CdTe. (c) Corresponding

AFM deflection-error image of Cl-treated CdTe. (d) Corresponding C-AFM current mapping image of the Cl-treated CdTe with 0 V tip DC voltage and illuminated by a LED with energy density of 12 mW/cm^2. The tip spring constant was 2800 N/m. The scale bar is 500 nm.

To observe the effect of large-angle GBs on current transport in Type-4 grains, we obtained CdTe films with mostly Type-4 grains by alternating the Cl treatment conditions. To investigate current characteristics of Type-4 grains, C-AFM study was carried out under light to enhance the induced current value of Type-4 grains. A homemade white LED was used to illuminate the device through the glass side with the apparatus shown in Fig. S9. The light density of the LED was 12 mW/cm^2 (the designed maximum output power of the LED), about one tenth the intensity of 1 Sun. No DC voltage was applied on the tip during the C-AFM scan under light. The false in the AFM height-sensor and corresponding AFM deflection-error images of Cl-treated CdTe shown in Fig. S9 is due to the out-of-flatness of the home-made LED lighter. The CSL TBs are seen in the height-sensor and AFM deflection-error images (Fig. S9b-c). From the C-AFM current mapping image (Fig. S9d), currents are larger at GBs and TBs under illumination than at similar locations without intentional illumination. Therefore, by applying illumination to the CdTe device, enhanced current transport resulting from GBs (including TBs) is clearly seen in the Type-4 CdTe grains. During this process, the homemade LED played a crucial role, because no current was observed without the applied LED light. Compared with Type-1, -2, and -3 grains, Type-4 grains show larger resistance. Thus, for Type-4 grains, the enhanced current transport of the GBs must be studied under a higher intensity of illumination than that of Type-1, -2, and -3 grains. Therefore, Type-4 grains are likely a limitation for current transport, which should be avoided through device fabrication processes.

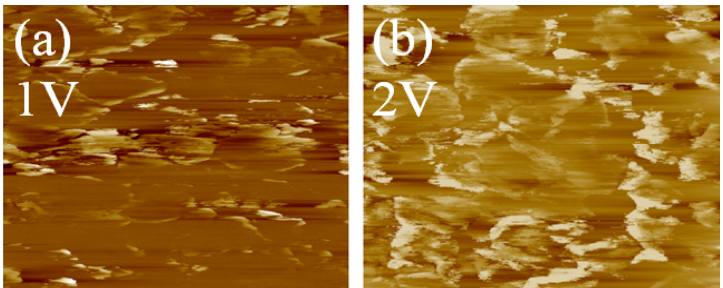

Fig. S10. Conductive atomic force microscopy (C-AFM) current mapping images of Cl-treated and Cu-incorporated CdTe with different tip DC bias voltages. (a) + 1 V, (b) + 2 V, (c) + 3 V, and (d) + 4 V. The scale bar is 1 μm.

We conducted C-AFM measurements with different tip DC voltages for Type-4 grains under illumination. To obtain sufficiently high currents that can be detectable by the C-AFM system, a tip DC bias larger than the open circuit voltage of solar cells must be applied. Fig. S10 illustrates the C-AFM current images of CdTe polycrystalline thin films without TBs with 1 V to 4 V of tip DC voltage. The conductive area appears at the GBs with 1 V of applied tip DC voltage. The conductive area is gradually broadened with the increase of tip DC voltage. When the tip DC voltage is 4 V, the entire grain interior becomes a high-current conductive area. With the increase of tip DC bias, the conductive region greatly extended from the GBs to grain interiors (Fig. S10). This may be due to the potential difference between GBs and grain interiors. The tip DC voltage gradually overcame the potential difference between GBs and grain interiors.

Electron beam induced current results: We acquired EBIC measurements on cross-sections of CdTe solar cells devices (Fig. S11). Fig. S11a shows the CdTe cross-section SEM image. Fig. S11b shows the electron-beam-induced current (EBIC) image of CdTe solar cells with Cu/Au back contacts. Bright and dark regions are well distinguished in the EBIC mapping image, with the bright regions representing larger currents. Combined with the SEM image

and EBIC images, the bright regions are seen to correspond to GBs of CdTe polycrystalline thin films. The cross-section was fabricated by mechanically cleaving the glass substrate. The EBIC current mapping reflects the carrier collection efficiency determined by localized electric fields and recombination rates. Combined with the SEM and EBIC mapping images (Fig. S11), these images reveal that GBs are more efficient in carrier collection than the grain interiors, which is largely consistent with the C-AFM results. The strong EBIC enhancement can be attributed either to local built-in electric fields at the GBs, and/or to a reduced recombination rate. The current region would not change if the strong current in the GBs and TBs was induced by a reduced recombination rate in the C-AFM current mapping image. Thus, the high current area enlarges with the increase of the tip DC voltage, indicating a localized field near GBs.

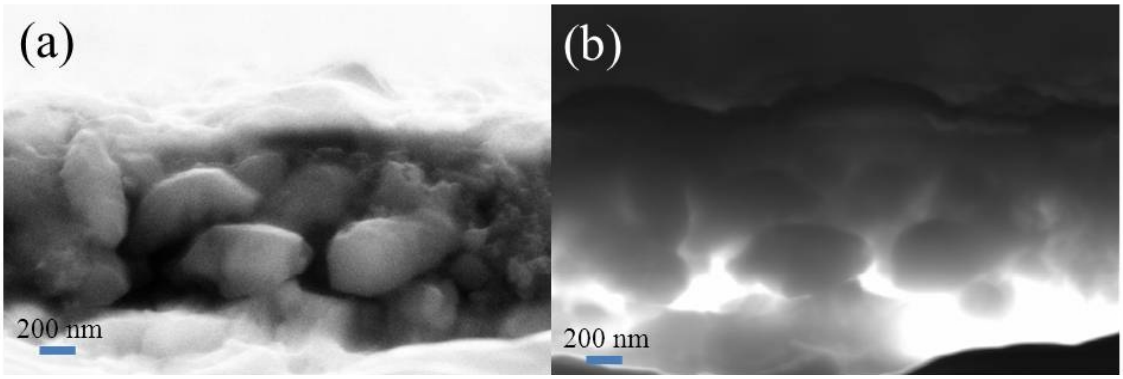

Fig. S11. (a) Scanning electron microscopy (SEM) image of the cross-section of a CdTe solar cell. (b) Electron-beam-induced current (EBIC) image of a CdTe solar cell.

CAFM current mapping and scanning Kelvin probe microscopy results of as-grown CdTe: Fig. S12 shows an AFM height-sensor image and an SKPM image of as-grown CdTe. The results indicate that the grain interior of as-grown CdTe shows a higher potential than that of the GBs. Fig. S13 shows the AFM height-sensor image, C-AFM current mapping image,

and AFM deflection-error image of an as-grown CdTe polycrystalline thin film. The as-grown CdTe also clearly shows GB-enhanced current transport phenomena.

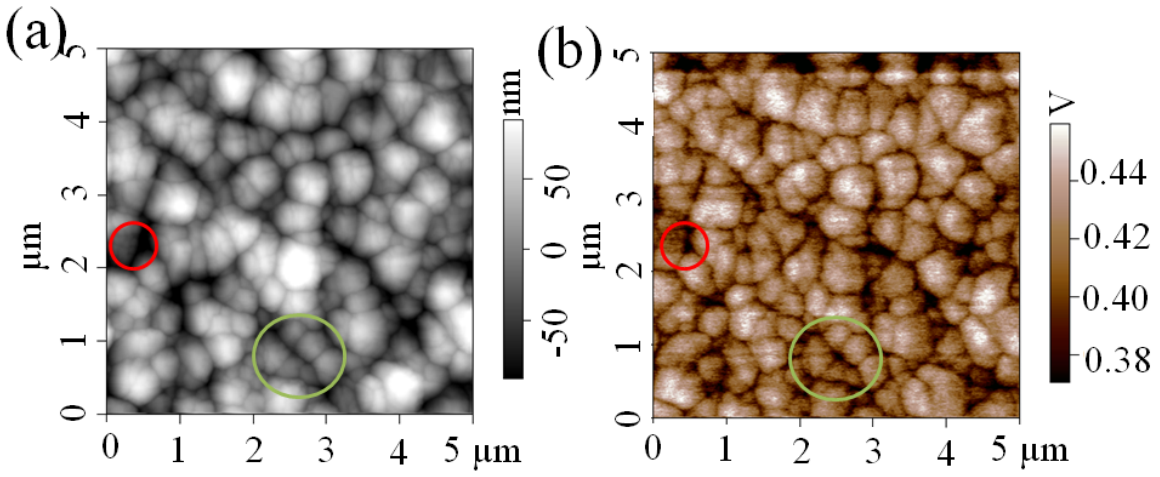

Fig. S12. (a) Atomic force microscopy (AFM) height-sensor image of as-grown CdTe. (b) Scanning Kelvin probe microscopy (SKPM) image of as-grown CdTe.

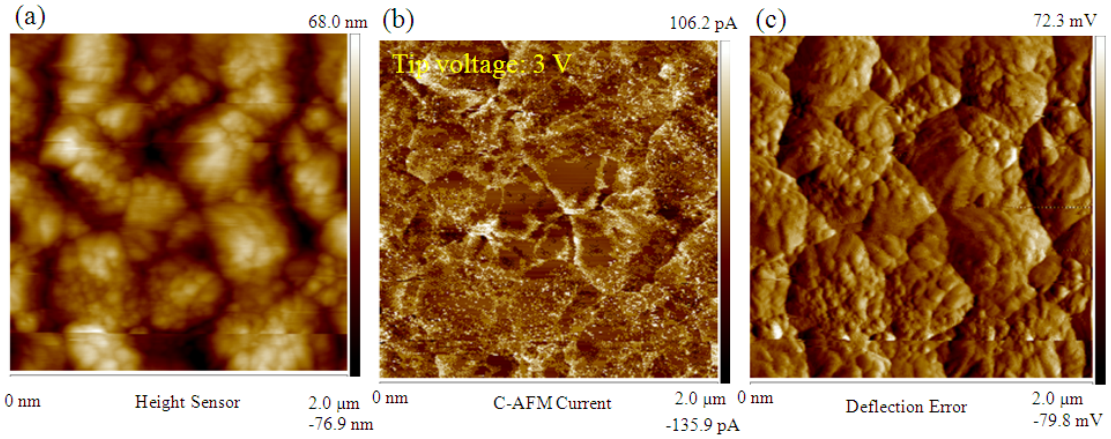

Fig. S13. (a) Atomic force microscopy (AFM) height-sensor image of as-grown CdTe surface without Cl treatment and Cu incorporation. (b) Conductive-AFM (C-AFM) current image of as-grown CdTe surface without Cl treatment and Cu incorporation, and with a 3 V tip DC voltage and no light. (c) AFM deflection-error image of as-grown CdTe surface without Cl treatment and Cu incorporation.

References:

1. Sascha Sadewasser, Thilo Glatzel, Kelvin Probe Force Microscopy, Springer, P13.